

Densities, Viscosities, and Self-Diffusion Coefficients of Aqueous Mixtures of NaBH_4 , NaB(OH)_4 , and NaOH Using the BH_4^- Delft Force Field (DFF/ BH_4^-)

Postma, Julien R.T.; Habibi, Parsa; Dey, Poulumi; Vlugt, Thijs J.H.; Moulτος, Othonas A.; Padding, Johan T.

DOI

[10.1021/acs.jced.4c00629](https://doi.org/10.1021/acs.jced.4c00629)

Publication date

2025

Document Version

Final published version

Published in

Journal of Chemical and Engineering Data

Citation (APA)

Postma, J. R. T., Habibi, P., Dey, P., Vlugt, T. J. H., Moulτος, O. A., & Padding, J. T. (2025). Densities, Viscosities, and Self-Diffusion Coefficients of Aqueous Mixtures of NaBH_4 , NaB(OH)_4 , and NaOH Using the BH_4^- Delft Force Field (DFF/ BH_4^-). *Journal of Chemical and Engineering Data*, 70(5), 1830-1842. <https://doi.org/10.1021/acs.jced.4c00629>

Important note

To cite this publication, please use the final published version (if applicable).
Please check the document version above.

Copyright

Other than for strictly personal use, it is not permitted to download, forward or distribute the text or part of it, without the consent of the author(s) and/or copyright holder(s), unless the work is under an open content license such as Creative Commons.

Takedown policy

Please contact us and provide details if you believe this document breaches copyrights.
We will remove access to the work immediately and investigate your claim.

Densities, Viscosities, and Self-Diffusion Coefficients of Aqueous Mixtures of NaBH_4 , NaB(OH)_4 , and NaOH Using the BH_4^- Delft Force Field (DFF/ BH_4^-)

Julien R. T. Postma, Parsa Habibi, Poulumi Dey, Thijs J. H. Vlugt, Othonas A. Moulton, and Johan T. Padding*

Cite This: *J. Chem. Eng. Data* 2025, 70, 1830–1842

Read Online

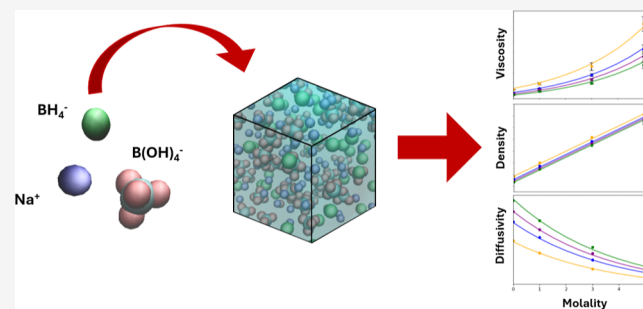
ACCESS |

Metrics & More

Article Recommendations

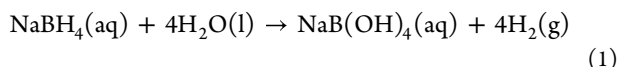
Supporting Information

ABSTRACT: One of the most promising energy carriers for transport applications are hydrogen-based energy carriers. NaBH_4 is a hydrogen energy carrier and produces hydrogen bubbles when it is dissolved in water. The formation of hydrogen bubbles hinders experimental measurements of the thermodynamic and transport properties of aqueous NaBH_4 solutions at elevated temperatures. Accurate knowledge of these properties is essential for the NaBH_4 hydrolysis reactor modeling and design. Molecular dynamics (MD) simulations provide the option to study the thermodynamic and transport properties of NaBH_4 aqueous solutions without hindering hydrogen bubble formation. In this work, a new force field is developed for BH_4^- , namely, the Delft force field of BH_4^- (DFF/ BH_4^-), which, combined with additional force fields, can accurately describe experimental densities and viscosities of 0 to 5 m (mol salt/kg water) NaBH_4 , 0 to 3 m NaB(OH)_4 , and 1 m NaOH aqueous solutions at 295 K within 1.8% and 10.8% maximum deviation, respectively. Empirical fitting correlations are created for densities, viscosities, and self-diffusivities obtained from the MD simulations of 0 to 5 m NaBH_4 , 0 to 5 m NaB(OH)_4 , and 0 to 1 m NaOH aqueous solutions at 295–363 K for NaBH_4 hydrolysis reactor modeling and design purposes.



INTRODUCTION

Hydrogen-based energy carriers are investigated as one of the options to reduce greenhouse gas (GHG) emissions.^{1–8} Hydrogen gas has a high gravimetric energy density of 120 to 142 MJ/kg and is therefore a prime candidate as an alternative energy carrier.^{8–12} Unfortunately, the volumetric energy density of gaseous or liquefied hydrogen is limited, which is why there is an increased interest in alternatives that offer higher volumetric energy densities such as solid hydrogen carriers.^{8,13–17} NaBH_4 is considered one of the most promising solid hydrogen carriers with a high gravimetric hydrogen capacity of 10.7 wt %.^{8,18–23} NaBH_4 reacts with H_2O to create hydrogen gas and the side product NaB(OH)_4 , following Reaction 1.^{24–26} The reaction rate of Reaction 1 can be enhanced using a catalyst (based on Ru, Pt, Co, or Ni).^{18,27–30}



For NaBH_4 , a potential use has been found in different transport applications (vehicles, small apparatuses, and drones) as a hydrogen-based energy carrier, due to its stable and safe storage in the solid state.^{15,16,31–35} It should be noted that Reaction 1 is mainly considered for maritime applications³⁶ due to the continuous availability of water, utilizing reverse osmosis.^{37,38} Reverse osmosis enables the conversion of brine

to fresh water during the transport period, and hence, reducing the fuel weight requirement at the start of transport.^{8,36,39,40}

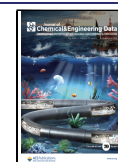
As NaBH_4 reacts with water, an aqueous mixture of NaBH_4 and NaB(OH)_4 is formed.^{27,29,41} Both the concentrations of NaBH_4 and NaB(OH)_4 change the thermodynamic and transport properties, such as density and viscosity, of aqueous solutions. Increasing the concentration of both NaBH_4 and NaB(OH)_4 by 5 m (mol salt/kg water) increases the viscosity by a factor of ca. 7, which influences the hydrodynamics of NaBH_4 hydrolysis reactors. To the best of our knowledge, limited information on thermodynamic and transport properties is available for aqueous solutions of NaBH_4 and mixtures of NaBH_4 with NaB(OH)_4 , even though these properties are crucial for performance optimization of NaBH_4 hydrolysis reactors. The lack of available property data is most likely due to the difficulty of obtaining reliable experimental data, while NaBH_4 reacts in aqueous solution. The reaction of NaBH_4 in

Received: November 1, 2024

Revised: April 2, 2025

Accepted: April 4, 2025

Published: April 18, 2025



aqueous solution forms hydrogen bubbles, which lead to inconsistencies in the experimental measurements of most thermodynamic and transport properties such as viscosity, density, and diffusivity.^{19,24,25,42–44} Experimental measurements at higher temperatures (323–363 K) will only increase in difficulty due to the increase in the NaBH_4 hydrolysis reaction rate and H_2 bubble formation.^{19,24,25,44} The NaBH_4 reaction and H_2 bubble formation can be reduced sufficiently with the addition of NaOH to the aqueous solution, according to Minkina et al.,⁴⁵ to measure thermodynamic and transport properties at lower temperatures (283–303 K) of NaBH_4 aqueous solutions.^{46,47} Obtaining thermodynamic and transport properties at varying temperatures and salt compositions will provide further insight into the NaBH_4 hydrolysis reactor and $\text{NaB}(\text{OH})_4$ crystallizer modeling and design.^{48–54} The thermodynamic and transport properties of NaBH_4 and $\text{NaB}(\text{OH})_4$ aqueous solutions without any bubbles have specific relevance in resolved multiphase computational fluid dynamics (CFD) simulations when the hydrogen bubbles and electrolyte solution are considered separately. Such resolved CFD simulations are urgently needed to understand and predict the interplay between hydrodynamics, mass and energy transfer, and reactions occurring in heterogeneously catalyzed systems. Furthermore, to predict the performance of a full NaBH_4 hydrolysis reactor system, it may be necessary to use effective mixture densities and viscosities of gas–liquid mixtures, which can also be found through resolved CFD simulations based on the results presented in this work.

Classical force field-based molecular dynamics (MD) simulations provide the solution to the bubble interference problem by not considering the chemical reaction of NaBH_4 with H_2O . For the MD simulations in this work, the Lennard-Jones (LJ) and electrostatic interactions are the only intermolecular interactions considered, while still providing accurate thermodynamic and transport properties of aqueous salt solutions compared with new experimental data at low temperatures (295 K).^{55–58} A force field for BF_4^- was recently developed by Núñez-Rojas et al.⁵⁹ for LiBF_4 in propylene carbonate solutions, with a similar tetrahedral structure as BH_4^- . The fluorine atom of the BF_4^- force field has similar LJ parameters ($\sigma = 4.47 \text{ \AA}$ and $\epsilon = 144.8 \text{ K}$) to the proposed LJ parameters of BH_4^- , which is most likely due to the similarities in size. A force field for NaBH_4 was already developed by Li,⁶⁰ but this force field describes interactions of BH_4^- and Na^+ with H_2O in the gaseous phase and the NaBH_4 (and $\text{NaBH}_4 \cdot 2\text{H}_2\text{O}$) crystal geometry, density, and compressibility in the solid state. Furthermore, the force field developed by Li⁶⁰ is not a LJ and partial charge force field and is therefore not considered comparable or compatible with the force field developed in this work. Hence, currently no force field is available for BH_4^- anions in aqueous solutions. In this work, a new classical force field is developed for NaBH_4 and compared with new experimental density and viscosity data at low temperatures and stabilized alkaline conditions. The force field is combined with the DFF/ $\text{B}(\text{OH})_4^-$ force field⁵⁶ and compared with new experimental density and viscosity data at low temperatures and stabilized alkaline conditions. Densities, viscosities, and self-diffusivities of NaBH_4 and $\text{NaB}(\text{OH})_4$ aqueous solutions are computed at varying temperatures and salt compositions, based on expected hydrolysis reactor operating conditions (323–363 K and 1 bar). Empirical fitting correlations are created from the computed thermodynamic and transport properties of NaBH_4 , $\text{NaB}(\text{OH})_4$ and NaOH aqueous

solutions, which can be used for modeling and design of NaBH_4 hydrolysis reactors.

EXPERIMENTAL METHOD

Solution Preparation. Experiments are performed to obtain thermodynamic and transport properties (density and

Table 1. Details of All Species Used in the Experiments of This Work

component	chemical formula	CAS number	supplier	purity [%]
Milli-Q water	H_2O	7732-18-5		≥ 99.9
sodium hydroxide	NaOH	1310-73-2	Sigma-Aldrich	≥ 99.9
sodium metaborate tetrahydrate	$\text{NaBO}_2 \cdot 4\text{H}_2\text{O}$	10555-76-7	Thermo Fisher Scientific	≥ 98.5
sodium borohydride	NaBH_4	16940-66-2	CPH Chemicals	≥ 98.0

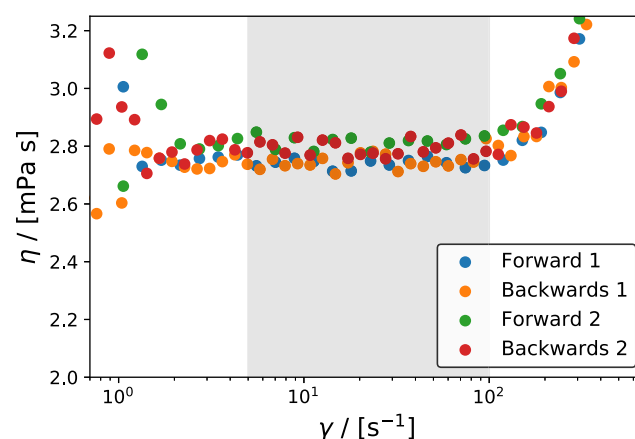
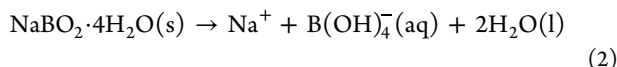


Figure 1. Viscosities (η) of NaBH_4 , NaOH , and $\text{NaB}(\text{OH})_4$ aqueous solutions vs shear rate (γ). The viscosity is measured using the MCR 320 rheometer with a 1 mm gap between the 50 mm diameter parallel plate and bottom plate to ensure low viscosity (close to 1 mPa s) stability. Four measurements are shown: two measurements with increasing shear rate as a function of time (i.e., Forward 1 and 2) and two measurements with decreasing shear rate (i.e., Backwards 1 and 2). The left part of the scatter curve shows low torque limits effects and the right part shows secondary flow effects. Both of these effects are common for plate rheometer measurements.⁶¹ In between these limits, the gray area, a stable viscosity value can be measured (2.77 mPa s in this measurement).

viscosity) of stable NaBH_4 aqueous solutions at ambient conditions (295 K and 1 bar pressure). NaOH is added to experimental aqueous solutions of NaBH_4 [and $\text{NaB}(\text{OH})_4$] to suppress the self-hydrolysis reaction of NaBH_4 (i.e., to prevent bubble formation) during the experimental measurements. All experimental aqueous solutions are stabilized with a 1 *m* NaOH (mol NaOH/kg water) concentration to obtain reliable and reproducible experimental data according to Minkina et al.⁴⁵ All solutions are prepared as follows. To stabilize the solution, NaOH is added to Milli-Q water first before adding NaBH_4 . The experimental solutions of NaBH_4 and NaOH have a concentration range of 0 to 5 *m* NaBH_4 with 1 *m* NaOH . The experimental mixture solutions of NaBH_4 , $\text{NaB}(\text{OH})_4$, and NaOH are made in a similar way as the NaBH_4 solutions, but in a concentration range of 1 to 3 *m* $\text{NaB}(\text{OH})_4$ with 1 *m* NaBH_4 and 1 *m* NaOH . The

experimental mixture solutions of NaBH₄, NaOH, and NaB(OH)₄ are made using solid NaBH₄, solid NaBO₂·4H₂O, solid NaOH, and Milli-Q water. The NaBO₂·4H₂O dissolves in water and forms NaB(OH)₄, as shown in Reaction 2. All materials used in the experiments can be found in Table 1. All experimental measurements are performed at a temperature of 295 K, and the composition of each solution is shown in Table 7.



Density and Viscosity Experiments. The densities of the experimental solutions are measured using an Anton Paar density meter DMA 5000. The viscosity is measured using an Anton Paar Modular Compact Rheometer (MCR) 302. The rheometer uses a stainless steel parallel-plate geometry for the rotating top and a steady stainless steel bottom. The spacing between the plates is 1 mm and is entirely filled with the selected solution. The bottom and top are both heated to 295 K. After the desired temperature is reached, the top plate is rotated with a logarithmically increasing shear rate from 0.1 to 1000 s⁻¹ (forward measurement), followed by a logarithmically decreasing shear rate from 1000 to 0.1 s⁻¹ (backward measurement). All equipment used for the density and viscosity measurements is first calibrated with pure water and compared with literature values at a temperature of 295 K. Figure 1 shows a typical example of two separate forward (increasing shear rate) and backward (decreasing shear rate) viscosity measurements for a mixture of 1 *m* NaOH, 1 *m* NaBH₄, and 2 *m* NaB(OH)₄ aqueous solution. At low shear rates (ca. 0.1 to 5 s⁻¹), the measurements show fluctuating results due to low torque limit effects.⁶¹ At medium shear rates (ca. 5 to 100 s⁻¹), the gray area, the fluctuations are reduced significantly and provide a stable measurement for the viscosity of the sample. At high shear rates (ca. 100 to 1000 s⁻¹), the apparent solution viscosity increases with shear rate due to secondary flow effects.⁶¹ All viscosity measurements can be found in the Supporting Information Figure S1.

SIMULATION METHOD

Force Fields. H₂O is modeled using the four-site rigid TIP4P/2005⁶² force field which accurately captures the

Table 2. Force Field Parameters for BH₄^{-a}

force field	$q_{\text{BH}_4^-}$ [<i>e</i>]	$\epsilon_{\text{BH}_4^-}/k_{\text{B}}$ [K]	$\sigma_{\text{BH}_4^-}$ [Å]
DFF/BH ₄ ⁻	0.85	148	4.50

^aThe BH₄⁻ ion is modeled as a single interaction site in which all the hydrogen atoms are positioned inside the boron atom. BH₄⁻ has a total charge of 0.85 ($q_{\text{BH}_4^-}$), which is based on the charge scaling of Madrid-2019⁵⁸ (0.85). The LJ energy parameter $\epsilon_{\text{BH}_4^-}$ is based on the LJ energy parameter of CH₄ by Martin and Siepmann.⁷⁵ The values of ϵ and σ for all combinations with BH₄⁻ follow the Lorentz–Berthelot mixing rules.^{76,77}

density, diffusivity, and viscosity of pure H₂O for a wide range of conditions.^{63–68} This force field is suitable not only for pure water, but also for salt solutions, such as NaCl,⁵⁷ NaOH,⁵⁵ and NaB(OH)₄⁵⁶ solutions, at varying concentrations, pressures and temperatures. Na⁺ is described using the Madrid-2019⁵⁸ force field, which has a charge scaling of 0.85. Charge scaling was first proposed by Leontyev and

Table 3. Details of All Species Used in the MD Simulations of This Work

component	chemical formula	CAS number	force field
water	H ₂ O	7732-18-5	TIP4P/2005 ⁶²
sodium	Na ⁺	7440-23-5	Madrid-2019 ⁵⁸
hydroxide	OH ⁻	14280-30-9	DFF/OH ⁻ force field ⁵⁵
tetrahydroxyborate	B(OH) ₄ ⁻	15390-83-7	DFF/B(OH) ₄ ⁻ force field ⁵⁶
borohydride	BH ₄ ⁻	16971-29-2	DFF/BH ₄ ⁻ force field

Table 4. Number of Water, Na⁺, BH₄⁻, and OH⁻ Molecules Used in the MD Simulations for Mixture Type 1^a

m_{NaBH_4}	m_{NaOH}	$N_{\text{H}_2\text{O}}$	N_{Na^+}	$N_{\text{BH}_4^-}$	N_{OH^-}	$\langle V \rangle$
1	1	1000	36	18	18	30,790
3	1	1000	72	54	18	32,972
5	1	1000	108	90	18	35,187

^a m_x is in mol of ion *x*/kg water and *V* is the average volume of the simulation in units of Å³. All simulations are run at 1 bar and 295 K and are used for optimization of the force field to minimize deviation from the experimental densities and viscosities at different concentrations of NaBH₄ and 1 *m* NaOH.

Stuchebrukhov,^{69–74} and it provides a simple way to correct for polarization effects in aqueous electrolyte solutions at the cost of less accurate predictions of properties such as free energies of hydration.^{56,64–66} B(OH)₄⁻ is modeled using the DFF/B(OH)₄⁻⁵⁶ model with a charge scaling of 0.85. The DFF/B(OH)₄⁻ model with a charge scaling of 0.85 *e* can accurately predict densities and viscosities of NaB(OH)₄ aqueous solution in the 0 to 5 *m* concentration range. OH⁻ is modeled using the Delft force field of OH⁻ (DFF/OH⁻) model,⁵⁵ with a charge scaling of 0.85. The DFF/OH⁻ model yields accurate densities and viscosities values within the 0 to 3 *m* NaOH concentration range in aqueous solution.

The DFF/BH₄⁻ model is developed in this work, and the optimized LJ interaction parameters and charges can be found in Table 2. The DFF/BH₄⁻ model has a single interaction site, similar to the TraPPE CH₄ force field.⁷⁵ Due to the low atomic mass of hydrogen compared to boron, the lack of hydrogen bond interactions with the hydrogen atom, and the decrease in computational demand, a single interaction site is considered sufficient for the simulation of BH₄⁻. The DFF/BH₄⁻ model is optimized using experimental densities and viscosities for varying concentrations of NaBH₄ at 295 K and 1 *m* NaOH aqueous solutions. All force field parameters [TIP4P/2005⁶² water force field, Madrid-2019⁵⁸ Na⁺ force field, DFF/OH⁻ force field,⁵⁵ DFF/B(OH)₄⁻ force field⁵⁶ and the BH₄⁻ force field developed in this work] used in this study are shown in Tables S1–S5 of the Supporting Information and the CAS-numbers can be found in Table 3.

All molecules and ions are considered rigid and follow the Lorentz–Berthelot mixing rules except for the Na⁺/–O_w and B(OH)₄⁻/–O_w LJ interaction which are specified in Tables S2 and S5 of the Supporting Information.^{76,77}

Simulation Settings. All MD simulations in this work are performed with the open-source large-scale atomic/molecular massively parallel simulator (LAMMPS)⁷⁸ (version August 2018). Interactions between any pair of ions or (nonbonded) atoms are described by an LJ (12-6) term and an electrostatic term. The SHAKE⁷⁹ and Rigid Body⁸⁰ algorithms in

Table 5. Number of Water, Na⁺, B(OH)₄⁻, BH₄⁻, and OH⁻ Molecules Used in the MD Simulations for Mixture Type 2^a

m_{NaBH_4}	$m_{\text{NaB(OH)}_4}$	m_{NaOH}	$N_{\text{H}_2\text{O}}$	N_{Na^+}	$N_{\text{BH}_4^-}$	$N_{\text{B(OH)}_4^-}$	N_{OH^-}	$\langle V \rangle$
1	1	1	1000	54	18	18	18	31,761
1	2	1	1000	72	18	36	18	32,681
1	3	1	1000	90	18	54	18	33,633

^a m_x is in mol of ion x /kg water and V is the average volume of the simulation in units of Å³. All simulations are run at 1 bar and 295 K and are used for optimization of the force field to minimize deviation from the experimental densities and viscosities at different concentrations of NaB(OH)₄ with 1 m NaBH₄ and 1 m NaOH.

Table 6. Number of Water, Na⁺, B(OH)₄⁻, BH₄⁻, and OH⁻ Molecules Used in the MD Simulations for Mixture Type 3^a

m_{NaBH_4}	$m_{\text{NaB(OH)}_4}$	$N_{\text{H}_2\text{O}}$	N_{Na^+}	$N_{\text{BH}_4^-}$	$N_{\text{B(OH)}_4^-}$	$\langle V \rangle$
1	0	1000	18	18	0	31,371
1	1	1000	36	18	18	32,383
1	3	1000	72	18	54	34,394
1	5	1000	108	18	90	36,423
3	0	1000	54	54	0	33,603
3	1	1000	72	54	18	34,609
3	3	1000	108	54	54	36,621
3	5	1000	144	54	90	38,633
5	0	1000	90	90	0	35,858
5	1	1000	108	90	18	36,869
5	3	1000	144	90	54	38,864
5	5	1000	180	90	90	40,857

^a m_x is in mol of ion x /kg water and V is the average volume of the simulation in units of Å³. All simulations are run at 1 bar and 323–363 K and are used as input data for empirical correlations at different concentrations of NaB(OH)₄ and NaBH₄.

LAMMPS⁷⁸ are used to fix the bond lengths and bond angles of all molecules and ions in the MD simulations. The Rigid Body⁸⁰ algorithm is used to accommodate the addition of B(OH)₄⁻ ions and requires longer computation time. Therefore, only simulations which include B(OH)₄⁻ ions use the Rigid Body⁸⁰ algorithm. All other simulations use the SHAKE algorithm.⁷⁹ The particle–particle particle–mesh (PPPM)^{76,81–83} method is used to handle long-range electrostatic interactions (relative uncertainty of 10⁻⁵). A cutoff radius of 10 Å is applied to the LJ and real space contribution of the electrostatic interactions. Analytic tail-corrections are applied for computing energies and pressures in the LJ interactions beyond a cutoff radius of 10 Å. To integrate the equation of motion, the Verlet algorithm⁸⁴ is used with a time step of 1 fs. Periodic boundary conditions are imposed in all directions. To maintain constant pressure and temperature, the Nosé–Hoover thermostat and barostat^{76,85,86} are applied to all simulations with coupling constants of 100 and 1000 fs, respectively. The Nosé–Hoover algorithm is adjusted for rigid bodies, as proposed by Kamberaj.⁸⁷ The On-the-Fly Calculation of Transport Properties (OCTP)⁸⁸ plugin is used for computing the dynamic viscosities, densities, and self-diffusion coefficients of all species [H₂O, Na⁺, B(OH)₄⁻, BH₄⁻, OH⁻]. The initial configurations for each mixture type are created using PACKMOL⁸⁹ (v20.3.1). For each starting condition, the volume of the simulation box is determined by a 1 to 2 ns equilibration run in the isobaric-isothermal (NPT) ensemble, followed by a 1 to 2 ns production run (NPT ensemble) to obtain the average box size. This average box size is subsequently used in the canonical (NVT) ensemble to compute the properties mentioned before. The NVT ensemble includes a 1 ns equilibration run (NVT ensemble) and a 10 to

30 ns production run (NVT ensemble). Densities are calculated using the average box volume from the NPT simulations. OCTP uses the Einstein relations^{77,90–92} to compute the dynamic viscosities (shown in eq 3), which are not influenced by finite-size effects.^{93–96}

$$\eta_{\alpha\beta} = \lim_{t \rightarrow \infty} \frac{1}{2t} \frac{V}{k_B T} \langle \left(\int_0^t P_{\alpha\beta}(t') dt' \right)^2 \rangle \quad (3)$$

where η is the viscosity, t is time, k_B is Boltzmann's constant, T is temperature, and P represents the pressure tensor. Self-diffusivities for each ion/molecule are determined from the mean square displacements (MSD) (shown in eq 4).^{77,97–101}

$$D_{i,\text{self}}^{\text{MD}} = \lim_{t \rightarrow \infty} \frac{1}{6N_i t} \left\langle \sum_{j=1}^{N_i} (r_{j,i}(t) - r_{j,i}(0))^2 \right\rangle \quad (4)$$

where $D_{i,\text{self}}$ is the self-diffusion coefficient for molecule/ion type i , N_i is the number of molecules/ions of type i , and $r_{j,i}$ represents the (unfolded) position of the j -th molecule/ion of species i . Equations 3 and 4 are valid at time scales where the slope of the MSD as a function of time is 1 in a log–log plot. The self-diffusivities are corrected for finite size effects using the Yeh–Hummer^{94,102–104} correction, as shown in eq 5

$$D_{i,\text{self}} = D_{i,\text{self}}^{\text{MD}} + \frac{k_B T \xi}{6\eta L} \quad (5)$$

where η is the dynamic viscosity, which is not influenced by finite-size effects,^{93–96} L is the length of the (cubic) simulation box, and ξ is a dimensionless number equal to 2.837298 for a cubic simulation box. The DelftBlue supercomputer¹⁰⁵ is used for performing MD simulations.

Mixture Types. MD simulations are performed for the following three mixture types. Mixture type 1 consists of 1000 H₂O molecules with 18 to 108 Na⁺, 0 to 90 BH₄⁻, and 18 OH⁻ ions at 295 K and 1 bar, as shown in Table 4. The average box size $\langle V \rangle$ in units of Å³ is shown in Table 4 for each molality at 295 K and 1 bar. The MD simulations of mixture type 1 provide a comparable molality concentration range as applied in the NaBH₄ and NaOH aqueous solution experiments performed in this work.

Mixture type 2 consists of 1000 H₂O molecules with 54 to 90 Na⁺, 18 to 54 B(OH)₄⁻, 18 BH₄⁻, and 18 OH⁻ ions at 295 K and 1 bar, as shown in Table 5. The average box size $\langle V \rangle$ in units of Å³ is shown in Table 5 for each molality at 295 K and 1 bar. The MD simulations of mixture type 2 provide a comparable molality concentration range as applied in the NaBH₄, NaB(OH)₄, and NaOH aqueous solution experiments performed in this work.

Mixture type 3 consists of 1000 H₂O molecules with 18 to 180 Na⁺, 0 to 90 B(OH)₄⁻, and 18 to 90 BH₄⁻ at 323, 343, 353, and 363 K and 1 bar, as shown in Table 6. The average box size $\langle V \rangle$ in units of Å³ is shown in Table 6 for each molality at

323 K and 1 bar. The MD simulations of mixture type 3 provide a comparable molality concentration and temperature range as found in the operating conditions of NaBH_4 hydrolysis reactors.^{50,51,106}

RESULTS AND DISCUSSION

BH_4^- Force Field (DFF/ BH_4^-) Optimization. To obtain densities, viscosities, and self-diffusivities for NaBH_4 aqueous

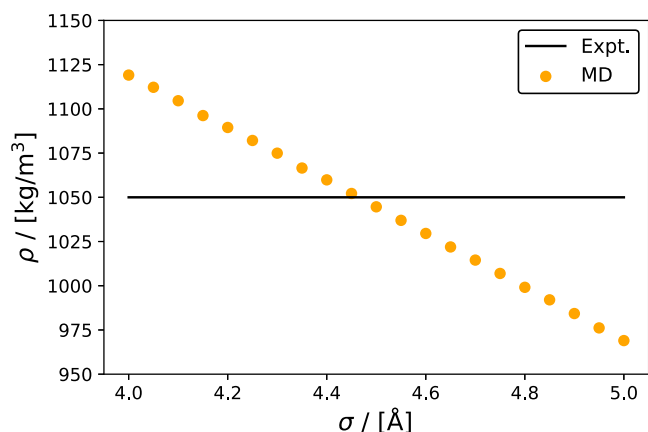


Figure 2. BH_4^- force field is optimized to match experimental density (ρ) measurements with the corresponding $\sigma_{\text{BH}_4^-}$ at 295 K and 1 bar. For the BH_4^- force field optimization, $\epsilon_{\text{BH}_4^-}/k_B$ and $q_{\text{BH}_4^-}$ are 148 K and 0.85 e , respectively. Both simulations and experiments use a 5 m concentration of NaBH_4 with 1 m NaOH in aqueous solution. The DFF/ BH_4^- force field is combined with TIP4P/2005⁶² water, Madrid-2019⁵⁸ Na^+ and DFF/ OH^- force field.⁵⁵ An acceptable deviation (within 1.5%) from the experimental density is found for $\sigma_{\text{BH}_4^-}$ between 4.45, 4.50, and 4.55 Å. The error bars for densities are smaller than the symbol size and have therefore been removed for clarity. The densities and density uncertainties of the MD simulations for each sigma can be found in Table S8.

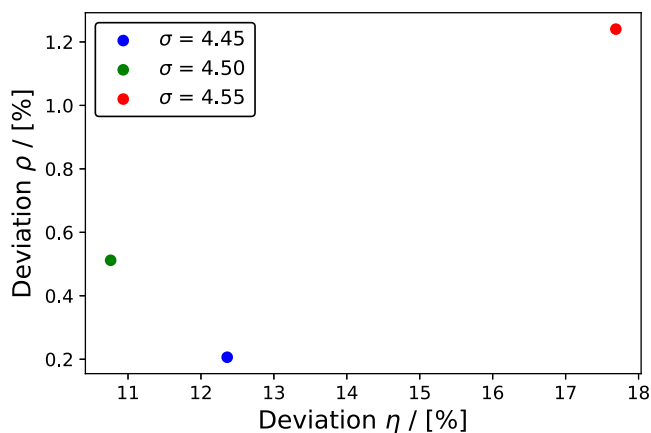


Figure 3. Deviations in density (ρ [%]) vs deviations in viscosity (η [%]) for experimental density and viscosity of 5 m [mol salt/kg water] NaBH_4 and 1 m NaOH in aqueous solution, compared to computed MD simulations of 5 m [mol salt/kg water] NaBH_4 and 1 m NaOH in aqueous solution at $\sigma = 4.45$ Å (blue), 4.50 Å (green), and 4.55 Å (purple). Force field parameters DFF/ BH_4^- are used for the simulations, combined with TIP4P/2005⁶² water, Madrid-2019⁵⁸ Na^+ and DFF/ OH^- force field.⁵⁵

solutions from MD simulations, a force field for BH_4^- is required. For the MD simulations in this work, the LJ and

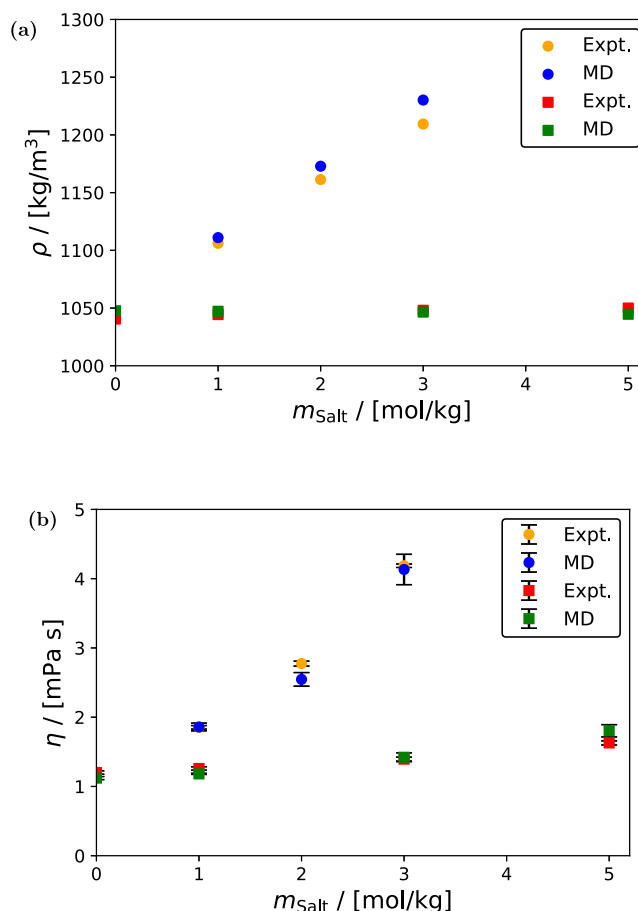


Figure 4. (a) Densities (ρ) and (b) viscosities (η) as a function of salt m [mol salt/kg water]. The square symbols (red: experiments, green: MD simulations) represent the densities and viscosities at different concentrations of NaBH_4 from 0 to 5 m [mol NaBH_4 /kg water] with 1 m NaOH in aqueous solution at 295 K and 1 bar. The circle symbols (yellow: experiments, blue: MD simulations) represent the densities and viscosities at different concentrations of NaB(OH)_4 from 1 to 3 m [mol NaB(OH)_4 /kg water] with 1 m NaBH_4 and 1 m NaOH in aqueous solution at 295 K and 1 bar. Force field parameters of DFF/ BH_4^- are used for the simulations, combined with the TIP4P/2005⁶² water, Madrid-2019⁵⁸ Na^+ , DFF/ B(OH)_4^- and DFF/ OH^- force field.⁵⁵ The error bars of viscosities for the experiments and MD simulations are presented as one standard deviation. The error bars for densities are smaller than the symbol size and have therefore been removed for clarity. The uncertainties of viscosity and density for experiments can be found in Table 7. Uncertainties for the MD simulations can be found in the Supporting Information Excel file provided.

electrostatic interactions are the only intermolecular interactions considered. For the MD simulations in this work, intramolecular interactions are not accounted for and a rigid structure is used. For both LJ and electrostatic interactions combined, three parameters can be used to optimize and tune the BH_4^- force field: σ (in units of Å), ϵ/k_B (in units of K), and q (in units of e). In this work, both q and ϵ/k_B are fixed to 0.85 e and 148 K, respectively. It should be noted that $q = 1$ is not considered in this work. In previous work, Joung–Cheatham developed a $q = 1$ nonpolarizable force field for NaCl , which was unsuccessful in simultaneously predicting both free energies of hydration and transport properties at higher molalities of NaCl .¹⁰⁷ Hence, to avoid this issue and maintain consistency in the Na^+ charge scaling in aqueous mixtures of

Table 7. Experimental Measurements of Density (ρ), One Standard Deviation of the Density Data (ρ_{error}), Viscosity (η), and One Standard Deviation of the Viscosity Data (η_{error}) for Different Concentrations of NaBH₄ and NaB(OH)₄ for Aqueous Solution of 1 *m* of NaOH Solutions at 295 K and 1 bar Pressure^a

molality NaB(OH) ₄ [<i>m</i> [mol salt/kg water]]	molality NaBH ₄ [<i>m</i> [mol salt/kg water]]	ρ [kg/m ³]	ρ_{error} [kg/m ³]	η [mPa s]	η_{error} [mPa s]
0	0	1040.5	0.078	1.20	0.024
0	1	1044.4	0.43	1.26	0.025
0	3	1048.1	0.50	1.39	0.029
0	5	1050.0	0.21	1.63	0.030
1	1	1106.1	0.097	1.85	0.025
2	1	1161.2	0.10	2.82	0.036
3	1	1209.4	0.14	4.19	0.025

^aDensities are measured using a DMA 5000 densitometer, and viscosity is measured with the MCR 320 rheometer. All solutions for these measurements are stabilized using 1 *m* of NaOH to prevent any hydrogen bubble formation during the measurements. The uncertainty of density (ρ_{error}) and viscosity (η_{error}) shown in this table are one standard deviation from the experimental data.

Na⁺, BH₄[−], OH[−], and B(OH)₄[−], the value of q is fixed at 0.85. The value of ϵ/k_B is fixed at 148 K to match the energy minimum of methane (CH₄), which has a similar structure and size to BH₄[−].⁷⁵ Therefore, the force field is exclusively optimized using σ to minimize the deviation from experimental densities and viscosities within the desired concentration range of NaBH₄ (0 to 5 *m* NaBH₄ in aqueous solution). It should be noted that ion pairing, salt clustering, and crystallization do not occur in any of our MD simulations, as shown by the radial distribution functions (RDFs) in Figure S4 of the Supporting Information, as the anions are only present outside the second hydration layer of Na⁺. If one would exclusively focus on the predicted density of a 5 *m* NaBH₄ with 1 *m* NaOH aqueous solution at 295 K, as used in the experiments, Figure 2 shows that the computed density has minimal deviation from the experimental density when σ is in the range of 4.45–4.55 Å (within 1.5% maximum deviation). The precise value of σ is chosen as a balance between matching the experimental density and matching the experimental viscosity of an aqueous solution of 5 *m* NaBH₄ with 1 *m* NaOH. Figure 3 shows that for all choices of σ within the range 4.45–4.55 Å, where the density deviation is acceptably small, the smallest viscosity deviation occurs at $\sigma = 4.50$. For the BH₄[−] force field, therefore, a σ of 4.50 Å is chosen due to having the best agreement with viscosity, while maintaining a density deviation below 1%. The BH₄[−] force field with a σ of 4.50 Å will be referred to as the DFF/BH₄[−] and is used for the MD simulations. Figure 4a,b shows the experimental densities and viscosities (red squares) compared with MD simulations (green squares) for aqueous solutions of 0 to 5 *m* NaBH₄ with 1 *m* NaOH. The DFF/BH₄[−] has maximum deviations for densities and viscosities of 0.7% and 10.8%, respectively, and average deviations of 0.4% and 6.4%, respectively, at 295 K compared with experimental data. The maximum deviation is defined as the largest deviation between a MD simulation compared with an experimental data point with a matching concentration, as shown in eq 6.

$$\sigma_{\text{max}} = \max_i \left(\left| 1 - \frac{n_{k,i}}{n_{l,i}} \right| \right) \quad (6)$$

where $n_{k,i}$ is the i th data point for data type k (MD simulations or empirical fit inputs) and $n_{l,i}$ is the i th data point for data type l (experiments or MD simulations). The absolute average deviation is defined as the average of all deviations for each MD simulation compared with their respected experimental data point, as shown in eq 7

$$\sigma_{\text{AA}} = \frac{1}{N} \sum_{i=1}^N \left| 1 - \frac{n_{k,i}}{n_{l,i}} \right| \quad (7)$$

where N is the size of the data set.

The self-diffusivity of BH₄[−] is compared with a single experiment by Wang et al.¹⁰⁸ for which the diffusion coefficient of $(1.62 \pm 0.05) \times 10^{-9}$ m²/s is measured with a concentration of 0.02 *m* NaBH₄ and 1 *m* NaOH at 303 K. A comparable BH₄[−] self-diffusion coefficient of $(1.82 \pm 0.16) \times 10^{-9}$ m²/s is found for simulations with a concentration of 0.11 *m* NaBH₄ and 1 *m* NaOH at 303 K after Yeh–Hummer correction. A concentration of 0.11 *m* of NaBH₄ is similar to adding two ions of BH₄[−] to a system of 1000 water molecules; hence, using fewer ions would not provide reliable results. It should be noted that the corrected self-diffusion is in agreement with the experiment of Wang et al.¹⁰⁸ at infinite dilutions conditions despite the force field not being optimized on the self-diffusion of BH₄[−].

Experimental Salt Mixtures Compared with MD. In the previous subsection, the DFF/BH₄[−] model was optimized using experimental aqueous solutions of NaBH₄ and NaOH. To use the DFF/BH₄[−] model for hydrolysis reaction conditions, the research is extended to aqueous solutions of NaBH₄, NaB(OH)₄, and NaOH. Several mixture compositions are prepared for a comparative study between experiments and MD simulations. The experimental densities and viscosities measured for aqueous mixtures of 0 to 3 *m* NaB(OH)₄, 1 *m* NaBH₄, and 1 *m* NaOH at 295 K and 1 bar, respectively, are shown in Table 7. Figure 4a,b shows the experimental densities and viscosities (yellow circles) compared with MD simulation (blue circles) for aqueous mixture solutions of 1 to 3 *m* NaB(OH)₄, 1 *m* NaBH₄, and 1 *m* NaOH. The experimentally measured mixture densities and viscosities (yellow) match the mixture MD simulations (blue) within 1.8% maximum deviation for density and 8.3% maximum deviation for viscosity. It should be noted that the maximum deviations for densities only increased from 0.7 to 1.8%, and for viscosities, the maximum deviation decreased from 10.8 to 8.3% when extending the force field capabilities to experimental mixture solutions, while none of the force fields are further tuned for mixture solutions. The increase in maximum deviation from 0.7% to 1.8% in density for the DFF/BH₄[−] is most likely caused by the accumulative deviations of all the additional force fields used in the mixture simulations. The maximum deviations of density and viscosity (1.8% and 10.8%) are similar to maximum deviations of densities and viscosities reported in other works (typically 0.5–2% and 5–

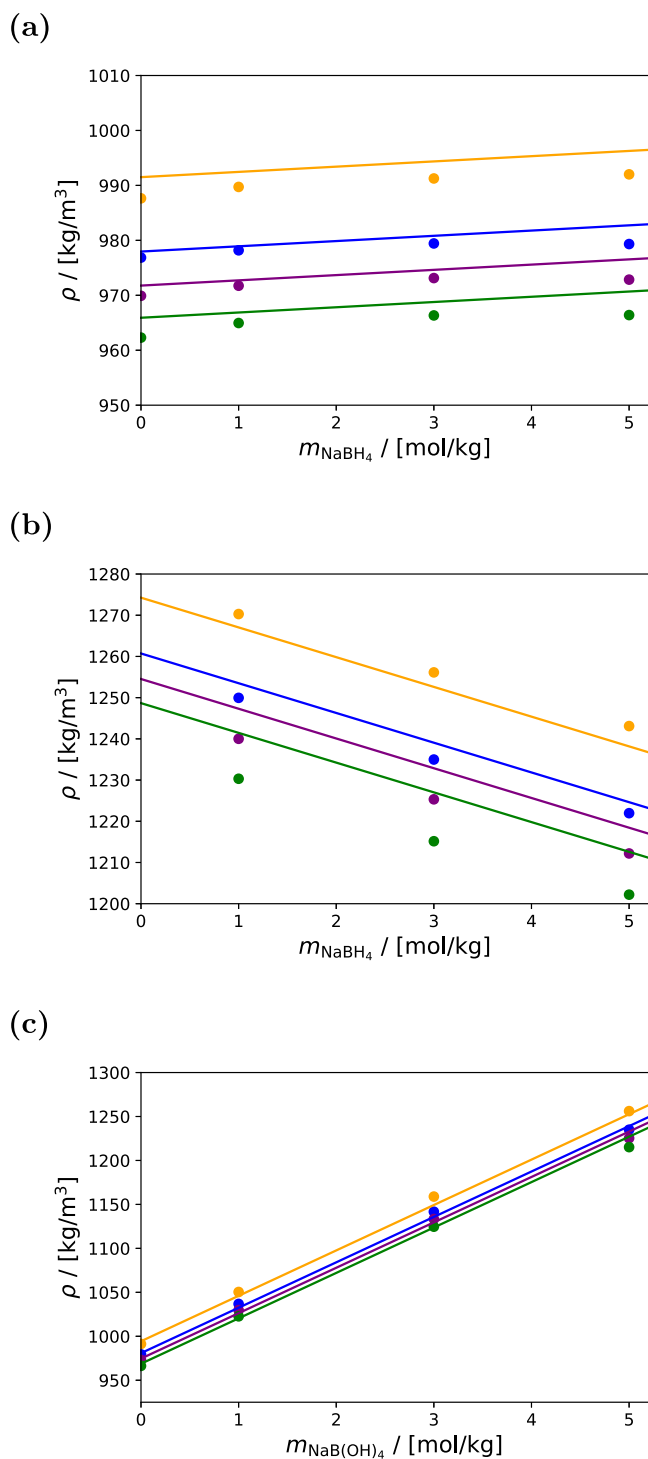


Figure 5. Computed densities (ρ) of NaBH_4 and NaB(OH)_4 aqueous solutions at 1 bar and 323 (yellow), 343 (blue), 353 (purple), and 363 (green) K are shown as circles in (a–c). (a) Densities for pure NaBH_4 aqueous solutions with the increasing NaBH_4 concentration at different temperatures. (b) Densities for NaBH_4 and NaB(OH)_4 aqueous solutions with a fixed NaB(OH)_4 concentration of 5 m and increasing NaBH_4 concentration at different temperatures. (c) Densities for NaBH_4 and NaB(OH)_4 aqueous solutions with a fixed NaBH_4 concentration of 3 m and increasing NaB(OH)_4 concentration at different temperatures. The empirical correlation is represented by solid lines and follows eq 8 with the parameters in Table 8. The error bars for densities are smaller than the symbol size and have therefore been removed for clarity. Uncertainties can be found in the Supporting Information Excel file provided.

Table 8. Density (ρ) Fitting Parameters of Eq 8 for NaBH_4 , NaB(OH)_4 , and NaOH Aqueous Solutions^a

dependency	parameter	value
n.a.	ρ_0	7.59×10^2 kg/m ³
NaB(OH)_4	A_1	5.66×10^1 kg/m ³ m ₁ ^{−1}
NaBH_4	A_2	9.54×10^{-1} kg/m ³ m ₂ ^{−1}
NaOH	A_3	4.24×10^1 kg/m ³ m ₃ ^{−1}
$\text{NaB(OH)}_4 \cdot \text{NaBH}_4$	A_4	-1.63×10^0 kg/m ³ m ₁ ^{−1} m ₂ ^{−1}
$\text{NaBH}_4 \cdot \text{NaOH}$	A_5	-2.53×10^0 kg/m ³ m ₂ ^{−1} m ₃ ^{−1}
T	A_6	7.50×10^4 kg/m ³ K

^aDensities are computed using MD simulations with the DFF/BH₄[−], the DFF/B(OH)₄[−],⁵⁶ Madrid-2019⁵⁸ Na⁺ force field, DFF/OH[−] force field,⁵⁵ and TIP4P/2005⁶² water. These fitting parameters are for the concentration and temperature range of 0 to 5 m NaBH_4 , 0 to 5 m NaB(OH)_4 , 0 to 1 m NaOH , and 295–363 K. m^{−1} is in units of kg water/mol salt.

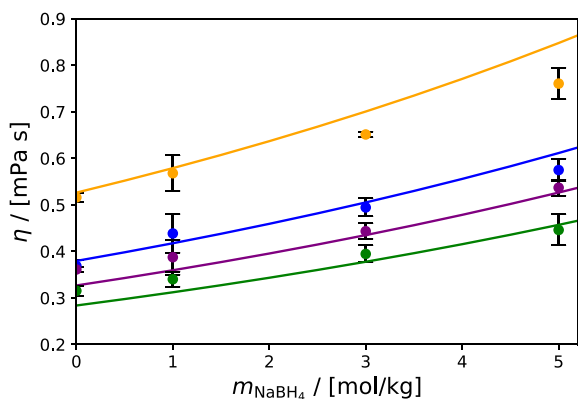
20%).^{55,56,109–113} Based on these results, the DFF/BH₄[−] force field, in combination with the other force fields [TIP4P/2005⁶² water force field, Madrid-2019⁵⁸ Na⁺ force field, DFF/OH[−] force field⁵⁵ and DFF/B(OH)₄[−] force field⁵⁶], is considered to be sufficiently accurate for concentrations of 0 to 5 m NaBH_4 , 0 to 5 m NaB(OH)_4 and 0 to 1 m NaOH and a temperature range from 295 to 363 K. Therefore, in the remainder of this work, we will focus on simulation results to formulate empirical correlations for densities, viscosities, and diffusion coefficients within the aforementioned concentration range.

Correlations for Salt Mixture Properties. For detailed reactor design purposes, a large data set of computed densities, viscosities, and self-diffusivities at different compositions of NaBH_4 and NaB(OH)_4 in aqueous solution is created at varying temperatures (323–363 K). All densities are computed from MD simulations for aqueous solutions of 1 to 5 m NaBH_4 and 0 to 5 m NaB(OH)_4 at different temperatures (323–363 K), as shown in Figure 5. It should be noted that the increase in the NaBH_4 concentration has an increasing and a decreasing effect on density depending on the absolute density value. This phenomenon is also found in experiments using a higher concentration of NaOH , as shown in Figure S3 of the Supporting Information. The following empirical correlation for the density has been created based on MD simulations data from different concentrations of 0 to 5 m NaBH_4 , 0 to 5 m NaB(OH)_4 , and 0 to 1 m NaOH in aqueous solutions at 295–363 K. The density at different temperatures is described using linear dependencies of concentrations and an inverse correlation for temperature, which is commonly used for density fitting of aqueous solutions.^{114,115}

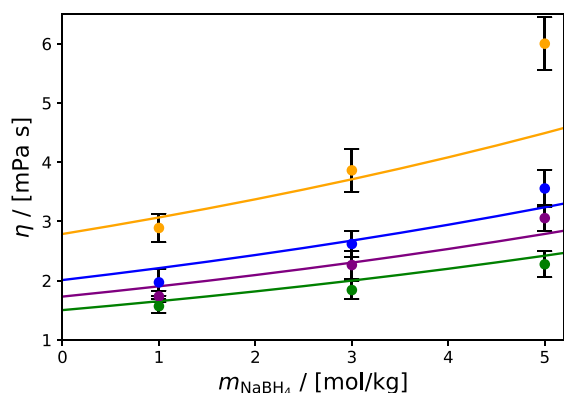
$$\rho = \rho_0 + A_1 m_1 + A_2 m_2 + A_3 m_3 + A_4 m_1 m_2 + A_5 m_2 m_3 + \frac{A_6}{T} \quad (8)$$

where m_1 , m_2 , and m_3 are the molalities (m) of NaB(OH)_4 , NaBH_4 , and NaOH , respectively, T is the absolute temperature, and ρ_0 and $A_1 \dots A_6$ are the density fitting parameters. The cross terms A_4 and A_5 for the molalities of NaB(OH)_4 and NaBH_4 and NaBH_4 and NaOH are added to describe the influence of NaBH_4 on the density of the aqueous solution. The molality of NaBH_4 will decrease the density of the

(a)



(b)



(c)

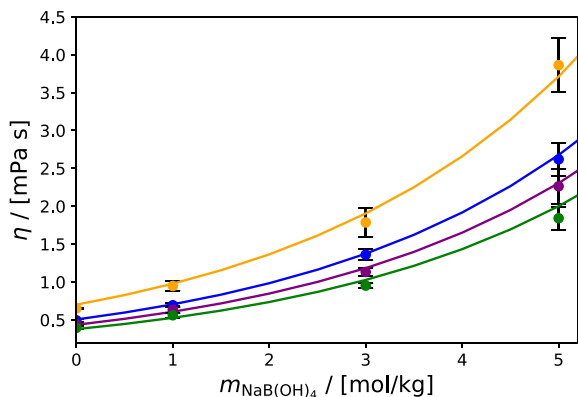


Figure 6. Computed viscosities (η) of NaBH_4 and NaB(OH)_4 aqueous solutions at 1 bar and 323 (yellow), 343 (blue), 353 (purple), and 363 (green) K are shown as circles in (a–c). (a) Viscosities for pure NaBH_4 aqueous solutions with the increasing NaBH_4 concentration at different temperatures. (b) Viscosities for NaBH_4 and NaB(OH)_4 aqueous solutions with a fixed NaB(OH)_4 concentration of 5 m and increasing NaBH_4 concentration at different temperatures. (c) Viscosities for NaBH_4 and NaB(OH)_4 aqueous solutions with a fixed NaBH_4 concentration of 3 m and increasing NaB(OH)_4 concentration at different temperatures. The empirical correlation is represented by solid lines and follows eq 9 with the parameters in Table 9. Uncertainties can be found in the Supporting Information Excel file provided.

Table 9. Viscosity (η) Fitting Parameters of Eq 9 for NaBH_4 , NaB(OH)_4 , and NaOH Aqueous Solutions^a

dependency	parameter	value	
n.a.	η_0	1.93×10^{-3}	mPa s
NaB(OH)_4	B_1	3.34×10^{-1}	m_1^{-1}
NaBH_4	B_2	9.54×10^{-2}	m_2^{-1}
NaOH	B_3	2.49×10^{-1}	m_3^{-1}
T	B_4	1.81×10^3	K

^aViscosities are computed using MD simulations with the DFF/ BH_4^- , the DFF/ B(OH)_4^- ,⁵⁶ Madrid-2019⁵⁸ Na^+ force field, DFF/ OH^- force field,⁵⁵ and TIP4P/2005⁶² water. These fitting parameters are for the concentration and temperature range of 0 to 5 m NaBH_4 , 0 to 5 m NaB(OH)_4 , 0 to 1 m NaOH , and 295–363 K. m^{-1} is in units of kg water/mol salt.

aqueous solution when the overall density is above a threshold (approximately 1000 kg/m³). Similarly, the molality of NaBH_4 will increase the density of the aqueous solution when the overall density is below the threshold. This same behavior is also found in the density experiments with higher concentrations of NaOH , as shown in Figure S3 in the Supporting Information. It should be noted that for all empirical correlations, the simulations for pure water, NaOH aqueous solutions, NaB(OH)_4 solutions in water and NaBH_4 with NaOH aqueous mixtures at varying temperatures (295–363 K) are included in the correlation. The fitting parameters for the empirical density correlation are listed in Table 8. This empirical density correlation has an average deviation of 0.4% from the MD simulations.

All viscosities are computed from MD simulations for aqueous solutions of 1 to 5 m NaBH_4 and 0 to 5 m NaB(OH)_4 at different temperatures (323–363 K), as shown in Figure 6. The following empirical correlation for viscosity has been created based on MD simulations data from different concentrations of 0 to 5 m NaBH_4 , 0 to 5 m NaB(OH)_4 , and 0 to 1 m NaOH aqueous solutions at 295–363 K. The viscosity at different concentrations and temperatures is described using an exponential correlation for concentration and temperature, which is commonly used for fitting viscosities of aqueous solutions.^{56,114,115}

$$\eta = \eta_0 \exp \left[B_1 m_1 + B_2 m_2 + B_3 m_3 + \frac{B_4}{T} \right] \quad (9)$$

where η_0 and $B_1 \dots B_4$ are the viscosity fitting parameters. No cross terms are added to the empirical viscosity fit since no inconsistencies are found for the viscosity relation between NaBH_4 , NaB(OH)_4 or NaOH molalities. The fitting parameters are listed in Table 9. The empirical correlation has an average deviation of 5.0% from the MD simulations.

All self-diffusivities of the BH_4^- are computed from MD simulations for aqueous solutions of 1 to 5 m NaBH_4 and 0 to 5 m NaB(OH)_4 at different temperatures (323–363 K), as shown in Figure 7. All values of self-diffusivity of BH_4^- are corrected for finite size effects using the Yeh–Hummer correction.^{94,102–104} The following empirical correlation for self-diffusivity of BH_4^- ($D_{\text{self},\text{BH}_4^-}$) has been created based on MD simulations data at different concentrations of 0.11 to 5 m NaBH_4 , 0 to 5 m NaB(OH)_4 , and 0 to 1 m NaOH aqueous solutions at 295–363 K. The self-diffusivity of BH_4^- at different concentrations and temperatures is described using an exponential correlation for concentration and temperature,

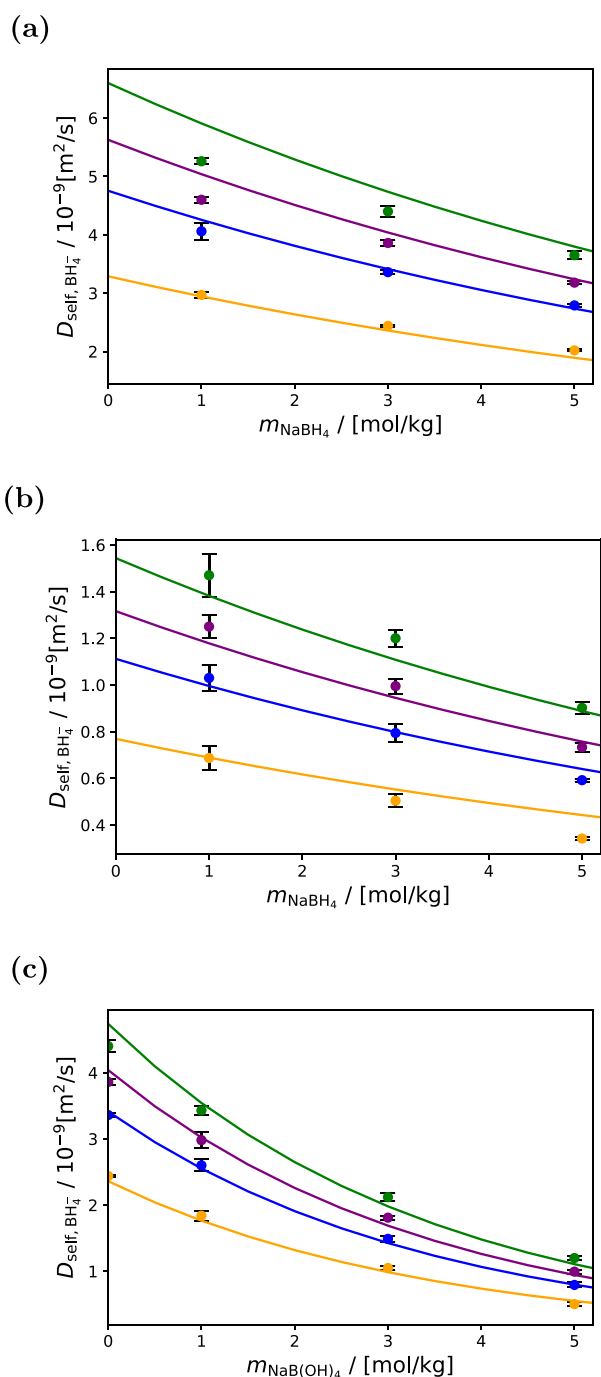


Figure 7. Computed self-diffusivities of BH_4^- ($D_{\text{self,BH}_4^-}$) for NaBH_4 and NaB(OH)_4 aqueous solutions at 1 bar and 323 (yellow), 343 (blue), 353 (purple), and 363 (green) K are shown as circles in (a–c). The self-diffusivities of BH_4^- are corrected for finite size effects using the Yeh–Hummer correction.^{94,102–104} (a) Self-diffusivities of BH_4^- for pure NaBH_4 aqueous solutions with increasing NaBH_4 concentration at different temperatures. (b) Self-diffusivities of BH_4^- for NaBH_4 and NaB(OH)_4 aqueous solutions with a fixed NaB(OH)_4 concentration of 5 m and increasing NaBH_4 concentration at different temperatures. (c) Self-diffusivity of BH_4^- for NaBH_4 and NaB(OH)_4 aqueous solutions with a fixed NaBH_4 concentration of 3 m and increasing NaB(OH)_4 concentration at different temperatures. The empirical correlation is represented by solid lines and follows eq 10 with the parameters in Table 10. The error bars for self-diffusivity of BH_4^- are presented as one standard deviation. Uncertainties can be found in the Supporting Information Excel file provided.

Table 10. Self-Diffusivity of BH_4^- ($D_{\text{self,BH}_4^-}$) Fitting Parameters of Eq 10 for NaBH_4 , NaB(OH)_4 , and NaOH Aqueous Solutions^a

dependency	parameter	value	
n.a.	$D_{\text{self},0}$	1.83×10^{-6}	m^2/s
NaB(OH)_4	C_1	-2.91×10^{-1}	m_1^{-1}
NaBH_4	C_2	-1.11×10^{-1}	m_2^{-1}
NaOH	C_3	-2.07×10^{-1}	m_3^{-1}
T	C_4	-2.04×10^3	K

^aSelf-diffusivities of BH_4^- are computed using MD simulations with the DFF/ BH_4^- , the DFF/ B(OH)_4^- ,⁵⁶ Madrid-2019⁵⁸ Na^+ force field, DFF/ OH^- force field,⁵⁵ and TIP4P/2005⁶² water. The self-diffusivities of BH_4^- are corrected for finite size effects using the Yeh–Hummer correction.^{94,102–104} These fitting parameters are for the concentration and temperature range of 0 to 5 m NaBH_4 , 0 to 5 m NaB(OH)_4 , 0 to 1 m NaOH , and 295–363 K. m^{-1} is in units of kg water/mol salt.

which is commonly used for self-diffusivity fitting of aqueous solutions.^{56,57}

$$D_{\text{self,BH}_4^-} = D_{\text{self},0} \exp \left[C_1 m_1 + C_2 m_2 + C_3 m_3 + \frac{C_4}{T} \right] \quad (10)$$

where $D_{\text{self},0}$ and $C_1 \dots C_4$ are the self-diffusivity fitting parameters. Also here, no cross terms are added to the empirical self-diffusivity fit since no inconsistencies are found for the self-diffusion relation between NaBH_4 , NaB(OH)_4 or NaOH molalities. The fitting parameters are listed in Table 10. The empirical correlation has an average deviation of 4.4% from the MD simulations.

CONCLUSIONS

The reactive nature of NaBH_4 in aqueous solution makes it difficult to experimentally determine thermodynamic and transport properties of aqueous NaBH_4 solutions, such as density and viscosity, especially at elevated temperatures. New experimental results for densities and viscosities are measured for 1–5 m NaBH_4 aqueous solutions, stabilized by 1 m of NaOH at 295 K. In this work, a new classical BH_4^- force field (DFF/ BH_4^-) is developed (combined with the TIP4P/2005⁶² water force field, Madrid-2019⁵⁸ Na^+ force field, and DFF/ OH^- force field⁵⁵) and optimized using the experimental results of stabilized NaBH_4 and NaOH aqueous solutions. The DFF/ BH_4^- force field can accurately describe the densities and viscosities of NaBH_4 and NaOH aqueous solutions, in the concentration range of 0 to 5 m of NaBH_4 and 1 m of NaOH at 295 K and 1 bar, within 0.7% and 10.8% maximum deviation, respectively. The applicability of the DFF/ BH_4^- force field is further tested with the addition of the DFF/ B(OH)_4^- force field⁵⁶ (in addition to the previously mentioned force fields) to the MD simulations. New experimental results for densities and viscosities are measured for 1–3 m NaB(OH)_4 , 1 m NaBH_4 , and 1 m NaOH stabilized aqueous solutions at 295 K. The combined force fields (TIP4P/2005⁶² water force field, Madrid-2019⁵⁸ Na^+ force field, DFF/ OH^- force field,⁵⁵ DFF/ BH_4^- force field, and DFF/ B(OH)_4^- force field⁵⁶) accurately describe the densities and viscosities of 0 to 3 m NaB(OH)_4 , 1 m NaBH_4 , and 1 m NaOH aqueous solutions at 295 K, within 1.8% and 8.3% maximum deviation, respectively. The MD simulations concentration and temperature range are extended to align with the expected application range of 0 to 5 m of NaBH_4 and 0 to 5 m of NaB(OH)_4 in

aqueous solutions at 323–363 K. Empirical correlations have been derived for densities, viscosities, and self-diffusivities using only MD simulations results in the concentration range of 0 to 5 *m* NaB(OH)₄, 0 to 5 *m* NaBH₄, and 0 to 1 *m* NaOH and a temperature range of 295–363 K. The empirical correlations derived in this work provide the thermodynamic and transport properties needed for the modeling and design of NaBH₄ hydrolysis reactors at varying temperatures and salt compositions. The data used for these empirical correlations can be found in the [Supporting Information Excel](#) file. It should be noted that the force fields used in this work [TIP4P/2005⁶² water force field, Madrid-2019⁵⁸ Na⁺ force field, DFF/OH[−] force field,⁵⁵ DFF/BH₄[−] force field, and DFF/B(OH)₄[−] force field⁵⁶ are only optimized within their respected concentration and temperature ranges. The empirical correlation for densities overestimates the simulation data for pure aqueous solutions at low temperatures to a maximum deviation of 1.32% [0 *m* NaBH₄ and 0 *m* NaB(OH)₄ at 298 K]. The empirical correlation for viscosities underestimates the simulation data at higher combined concentrations of NaBH₄ and NaB(OH)₄ at lower temperatures to a maximum deviation of 25.2% [5 *m* NaBH₄ and 5 *m* NaB(OH)₄ at 323 K]. The empirical correlation for self-diffusivities of BH₄[−] overestimates the simulation data at higher combined concentrations of NaBH₄ and NaB(OH)₄ at lower temperatures to a maximum deviation of 29.5% [5 *m* NaBH₄ and 5 *m* NaB(OH)₄ at 323 K]. It is not advised to use empirical correlations outside the recommended concentration and temperature range. It should be noted that NaB(OH)₄ has a higher influence on both densities and viscosities than NaBH₄, which makes the empirical correlation more suited for high concentrations of NaB(OH)₄ (more than 5 *m*) with lower concentrations of NaBH₄ (0 to 3 *m*) as shown in [Figure S2](#) of the Supporting Information. It should also be noted that the DFF/B(OH)₄[−] force field⁵⁶ is not optimized for higher concentrations of NaB(OH)₄ (more than 5 *m*). We recommend, for future research, expanding the DFF/BH₄[−] force field to cations such as K⁺ for applications of KBH₄ as another potential hydrogen carrier.

■ ASSOCIATED CONTENT

SI Supporting Information

The Supporting Information is available free of charge at <https://pubs.acs.org/doi/10.1021/acs.jced.4c00629>.

Force field parameters; viscosity measurements; computed MD simulations of viscosity for elevated (1–11 *m*) molalities (mol salt/kg water) of NaB(OH)₄ with 1 *m* NaBH₄ and 1 *m* NaOH at 353 K and 1 bar; computed densities and viscosities for the elevated molalities of NaB(OH)₄ with 1 *m* NaBH₄ and 1 *m* NaOH at 353 K and 1 bar; experimental densities (ρ) for different concentrations of NaOH, and NaBH₄ concentration in aqueous solution; experimental densities (ρ) and one standard deviation of the experimental densities (ρ_{error}) for different concentrations of NaBH₄ and NaOH in aqueous solution; MSD_{*D_i,self*} equation used for Figure S5 (eq S1); MSD_{*D_i,self*} equation used for Figure S5 (eq S2); RDFs *g*(*r*) versus radial distance [Å] for different ion and atom combinations with Na⁺ mean square displacement curves for calculating self-diffusivity and shear viscosity; and MD densities and one standard deviation for optimization of the DFF/BH₄[−] (PDF)

Sample simulation files for the MD simulations in LAMMPS software (ZIP)

All MD simulation data used for development of the empirical correlations of density, viscosity, and self-diffusivity (BH₄[−]) (corrected with Yeh–Hummer); all self-diffusivities of Na⁺ and H₂O and the self-diffusivities of Na⁺, BH₄[−] and H₂O which are not corrected for finite size effects (no Yeh–Hummer corrections); and uncertainties of densities (ρ_{error}), viscosities (η_{error}) and self-diffusivities *D_{i,error}* (Na⁺, BH₄[−] and H₂O) for all MD simulations (XLSX)

■ AUTHOR INFORMATION

Corresponding Author

Johan T. Padding – Complex Fluid Processing, Process & Energy Department, Faculty of Mechanical Engineering, Delft University of Technology, 2628 CB Delft, The Netherlands; orcid.org/0000-0003-4161-0748; Email: J.T.Padding@tudelft.nl

Authors

Julien R. T. Postma – Complex Fluid Processing, Process & Energy Department, Faculty of Mechanical Engineering, Delft University of Technology, 2628 CB Delft, The Netherlands

Parsa Habibi – Engineering Thermodynamics, Process & Energy Department, Faculty of Mechanical Engineering, Delft University of Technology, 2628 CB Delft, The Netherlands; Department of Materials Science and Engineering, Faculty of Mechanical Engineering, Delft University of Technology, 2628 CD Delft, The Netherlands

Poulumi Dey – Department of Materials Science and Engineering, Faculty of Mechanical Engineering, Delft University of Technology, 2628 CD Delft, The Netherlands; orcid.org/0000-0003-4679-1752

Thijs J. H. Vlugt – Engineering Thermodynamics, Process & Energy Department, Faculty of Mechanical Engineering, Delft University of Technology, 2628 CB Delft, The Netherlands; orcid.org/0000-0003-3059-8712

Othonas A. Moulton – Engineering Thermodynamics, Process & Energy Department, Faculty of Mechanical Engineering, Delft University of Technology, 2628 CB Delft, The Netherlands; orcid.org/0000-0001-7477-9684

Complete contact information is available at: <https://pubs.acs.org/doi/10.1021/acs.jced.4c00629>

Notes

The authors declare no competing financial interest.

■ ACKNOWLEDGMENTS

This work was supported by the project SH2IPDRIVE: Sustainable Hydrogen Integrated Propulsion Drives, funded by the RvO (reference number MOB21013), through the RDM regulations of Ministry of Economic Affairs and Climate Policy. This work was sponsored by NWO Domain Science for the use of supercomputer facilities. The authors acknowledge the use of computational resources of the DelftBlue supercomputer, provided by Delft High Performance Computing Centre (<https://www.tudelft.nl/dhpc>).

REFERENCES

- (1) Stančin, H.; Mikulčić, H.; Wang, X.; Duić, N. A review on alternative fuels in future energy system. *Renew. Sustain. Energy Rev.* **2020**, *128*, 109927.
- (2) Prasad, S.; Singh, A.; Joshi, H. C. Ethanol as an alternative fuel from agricultural, industrial and urban residues. *Resour. Conserv. Recycl.* **2007**, *50*, 1–39.
- (3) Sangeeta; Moka, S.; Pande, M.; Rani, M.; Gakhar, R.; Sharma, M.; Rani, J.; Bhaskarwar, A. N. Alternative fuels: An overview of current trends and scope for future. *Renew. Sustain. Energy Rev.* **2014**, *32*, 697–712.
- (4) Ramadhas, A. S. *Alternative Fuels for Transportation*; CRC Press, 2011.
- (5) Bouman, E. A.; Lindstad, E.; Rialland, A. I.; Strømman, A. H. State-of-the-art technologies, measures, and potential for reducing GHG emissions from shipping – A review. *Transp. Res. D Trans. Environ.* **2017**, *52*, 408–421.
- (6) Barreto, R. A. Fossil fuels, alternative energy and economic growth. *Econ. Modell.* **2018**, *75*, 196–220.
- (7) Ramesohl, S.; Merten, F. Energy system aspects of hydrogen as an alternative fuel in transport. *Energy Policy* **2006**, *34*, 1251–1259.
- (8) van Rheenen, E.; Padding, J.; Slootweg, C.; Visser, K. A review of the potential of hydrogen carriers for zero emission, low signature ship propulsion systems. 2021, <http://library.imarest.org/record/10649> (accessed June 30, 2023).
- (9) Dragan, M. Hydrogen Storage in Complex Metal Hydrides NaBH₄: Hydrolysis Reaction and Experimental Strategies. *Catalysts* **2022**, *12*, 356.
- (10) Qazi, U. Y. Future of Hydrogen as an Alternative Fuel for Next-Generation Industrial Applications; Challenges and Expected Opportunities. *Energies* **2022**, *15*, 4741.
- (11) Atilhan, S.; Park, S.; El-Halwagi, M. M.; Atilhan, M.; Moore, M.; Nielsen, R. B. Green hydrogen as an alternative fuel for the shipping industry. *Curr. Opin. Chem. Eng.* **2021**, *31*, 100668.
- (12) da Silva Veras, T.; Mozer, T. S.; da Costa Rubim Messeder dos Santos, D.; da Silva César, A. Hydrogen: Trends, production and characterization of the main process worldwide. *Int. J. Hydrogen Energy* **2017**, *42*, 2018–2033.
- (13) Abdelhamid, H. N. A review on hydrogen generation from the hydrolysis of sodium borohydride. *Int. J. Hydrogen Energy* **2021**, *46*, 726–765.
- (14) Marrero-Alfonso, E. Y.; Beaird, A. M.; Davis, T. A.; Matthews, M. A. Hydrogen generation from chemical hydrides. *Ind. Eng. Chem. Res.* **2009**, *48*, 3703–3712.
- (15) Hwang, H. T.; Varma, A. Hydrogen storage for fuel cell vehicles. *Curr. Opin. Chem. Eng.* **2014**, *5*, 42–48.
- (16) Sinigaglia, T.; Lewiski, F.; Santos Martins, M. E.; Mairesse Siluk, J. C. Production, storage, fuel stations of hydrogen and its utilization in automotive applications-a review. *Int. J. Hydrogen Energy* **2017**, *42*, 24597–24611.
- (17) Al-Zohbi, G.; Almoaikel, A.; Al-Shuhail, L. An overview on the technologies used to store hydrogen. *Energy Rep.* **2023**, *9*, 28–34.
- (18) Zou, Y. C.; Nie, M.; Huang, Y. M.; Wang, J. Q.; Liu, H. L. Kinetics of NaBH₄ hydrolysis on carbon-supported ruthenium catalysts. *Int. J. Hydrogen Energy* **2011**, *36*, 12343–12351.
- (19) Retnamma, R.; Novais, A. Q.; Rangel, C. M.; Yu, L.; Matthews, M. A. Kinetic modeling of self-hydrolysis of aqueous NaBH₄ solutions by model-based isoconversional method. *Int. J. Hydrogen Energy* **2014**, *39*, 6567–6576.
- (20) Mosier-Boss, P. A.; Becker, C. A.; Anderson, G. W.; Wiedemeier, B. J. Feasibility Studies of the NaBH₄/H₂O Hydrolysis to Generate Hydrogen Gas to Inflate Lighter than Air (LTA) Vehicles. *Ind. Eng. Chem. Res.* **2015**, *54*, 7706–7714.
- (21) Rusman, N. A.; Dahari, M. A review on the current progress of metal hydrides material for solid-state hydrogen storage applications. *Int. J. Hydrogen Energy* **2016**, *41*, 12108–12126.
- (22) Zhang, Q.; Mohring, R. M. Reaction chemistry between aqueous sulfuric acid and solid sodium borohydride. *Ind. Eng. Chem. Res.* **2009**, *48*, 1603–1607.
- (23) Hojjati-Najafabadi, A.; Aygun, A.; Tiri, R. N. E.; Gulbagca, F.; Lounissaa, M. I.; Feng, P.; Karimi, F.; Sen, F. Bacillus thuringiensis Based Ruthenium/Nickel Co-Doped Zinc as a Green Nanocatalyst: Enhanced Photocatalytic Activity, Mechanism, and Efficient H₂ Production from Sodium Borohydride Methanolysis. *Ind. Eng. Chem. Res.* **2023**, *62*, 4655–4664.
- (24) Andrieux, J.; Demirci, U. B.; Hannauer, J.; Gervais, C.; Goutaudier, C.; Miele, P. Spontaneous hydrolysis of sodium borohydride in harsh conditions. *Int. J. Hydrogen Energy* **2011**, *36*, 224–233.
- (25) Gonçalves, A.; Castro, P.; Novais, A. Q.; Rangel, C. M.; Matos, H. Modeling of catalytic hydrogen generation from sodium borohydride. *Comput.-Aided Chem. Eng.* **2008**, *25*, 757–762.
- (26) Stepanov, N.; Uvarov, V.; Popov, I.; Sasson, Y. Study of by-product of NaBH₄ hydrolysis and its behavior at a room temperature. *Int. J. Hydrogen Energy* **2008**, *33*, 7378–7384.
- (27) Ye, W.; Zhang, H.; Xu, D.; Ma, L.; Yi, B. Hydrogen generation utilizing alkaline sodium borohydride solution and supported cobalt catalyst. *J. Power Sources* **2007**, *164*, 544–548.
- (28) Wang, Y.; Hu, Z.; Chen, W.; Wu, S.; Li, G.; Chou, S. Non-Noble Metal-Based Catalysts Applied to Hydrogen Evolution from Hydrolysis of Boron Hydrides. *Small Struct.* **2021**, *2*, 2000135.
- (29) Brack, P.; Dann, S. E.; Wijayantha, K. G. U. Heterogeneous and homogenous catalysts for hydrogen generation by hydrolysis of aqueous sodium borohydride (NaBH₄) solutions. *Energy Sci. Eng.* **2015**, *3*, 174–188.
- (30) Li, Y.; Zhang, X.; Zhang, Q.; Zheng, J. B.; Zhang, N.; Chen, B. H.; Smith, K. J. Activity and kinetics of ruthenium supported catalysts for sodium borohydride hydrolysis to hydrogen. *RSC Adv.* **2016**, *6*, 29371–29377.
- (31) Demirci, U. B.; Akdim, O.; Andrieux, J.; Hannauer, J.; Chamoun, R.; Miele, P. Sodium borohydride hydrolysis as hydrogen generator: issues, state of the art and applicability upstream from a fuel cell. *Fuel Cells* **2010**, *10*, 335–350.
- (32) Kim, K.; Kim, T.; Lee, K.; Kwon, S. Fuel cell system with sodium borohydride as hydrogen source for unmanned aerial vehicles. *J. Power Sources* **2011**, *196*, 9069–9075.
- (33) Nunes, H. X.; Ferreira, M. J.; Rangel, C. M.; Pinto, A. M. Hydrogen generation and storage by aqueous sodium borohydride (NaBH₄) hydrolysis for small portable fuel cells (H₂ – PEMFC). *Int. J. Hydrogen Energy* **2016**, *41*, 15426–15432.
- (34) Sakamoto, Y.; Hoshi, N.; Murooka, S.; Cao, M.; Yoshizaki, A.; Hirata, K. Basic study on fuel-cell-hybrid-electric-vehicle fueled by sodium borohydride. In *The 2010 International Power Electronics Conference—ECCE ASIA*, 2010; pp 814–819.
- (35) Santos, D. M. F.; Sequeira, C. A. Sodium borohydride as a fuel for the future. *Renew. Sustain. Energy Rev.* **2011**, *15*, 3980–4001.
- (36) Kaya, C. Sodium Borohydride (NaBH₄) as a Maritime Transportation Fuel. *Hydrogen* **2024**, *5*, 540–558.
- (37) Malaeb, L.; Ayoub, G. M. Reverse osmosis technology for water treatment: State of the art review. *Desalination* **2011**, *267*, 1–8.
- (38) Peters, C. D.; Hankins, N. P. Osmotically assisted reverse osmosis (OARO): Five approaches to dewatering saline brines using pressure-driven membrane processes. *Desalination* **2019**, *458*, 1–13.
- (39) Lensing, D. A study on the integration of a novel NaBH₄ fueled hybrid system for a small inland vessel. Master Thesis, 2020.
- (40) van Nievelt, F. Maritime application of sodium borohydride as an energy carrier. Ph.D. Thesis, 2019.
- (41) Zhang, J. S.; Delgass, W. N.; Fisher, T. S.; Gore, J. P. Kinetics of Ru-catalyzed sodium borohydride hydrolysis. *J. Power Sources* **2007**, *164*, 772–781.
- (42) Churikov, A. V.; Gamayunova, I. M.; Zapsis, K. V.; Churikov, M. A.; Ivanishchev, A. V. Influence of temperature and alkalinity on the hydrolysis rate of borohydride ions in aqueous solution. *Int. J. Hydrogen Energy* **2012**, *37*, 335–344.
- (43) Moon, G. Y.; Lee, S. S.; Lee, K. Y.; Kim, S. H.; Song, K. H. Behavior of hydrogen evolution of aqueous sodium borohydride solutions. *J. Ind. Eng. Chem.* **2008**, *14*, 94–99.

- (44) Bartkus, T. P.; T'ien, J. S.; Sung, C. J. A semi-global reaction rate model based on experimental data for the self-hydrolysis kinetics of aqueous sodium borohydride. *Int. J. Hydrogen Energy* **2013**, *38*, 4024–4033.
- (45) Minkina, V. G.; Shabunya, S. I.; Kalinin, V. I.; Martynenko, V. V.; Smirnova, A. L. Stability of alkaline aqueous solutions of sodium borohydride. *Int. J. Hydrogen Energy* **2012**, *37*, 3313–3318.
- (46) Zhang, Q.; Wu, Y.; Sun, X.; Ortega, J. Kinetics of catalytic hydrolysis of stabilized sodium borohydride solutions. *Ind. Eng. Chem. Res.* **2007**, *46*, 1120–1124.
- (47) Wang, Q.; Zhang, L. F.; Zhao, Z. G. Hydrogen production by sodium borohydride in NaOH aqueous solution. *IOP Conf. Ser. Mater. Sci. Eng.* **2018**, *292*, 012031.
- (48) Kojima, Y.; Suzuki, K. I.; Fukumoto, K.; Kawai, Y.; Kimbara, M.; Nakanishi, H.; Matsumoto, S. Development of 10 kW-scale hydrogen generator using chemical hydride. *J. Power Sources* **2004**, *125*, 22–26.
- (49) Sousa, T.; Fernandes, V. R.; Pinto, P. J.; Slavkov, Y.; Bosukov, L.; Rangel, C. M. A sodium borohydride hydrogen generation reactor for stationary applications: Experimental and reactor simulation studies. *Chem. Eng. Sci.* **2012**, *84*, 70–79.
- (50) Zhang, J.; Zheng, Y.; Gore, J. P.; Fisher, T. S. 1 kWe sodium borohydride hydrogen generation system. Part I: Experimental study. *J. Power Sources* **2007**, *165*, 844–853.
- (51) Zhang, J.; Zheng, Y.; Gore, J. P.; Mudawar, I.; Fisher, T. S. 1 kWe sodium borohydride hydrogen generation system. Part II: Reactor modeling. *J. Power Sources* **2007**, *170*, 150–159.
- (52) Zaykovskaya, A.; Louhi-Kultanen, M. Cooling and Evaporative Crystallization of α -D-Galactose from a Highly Viscous Industrial Side Stream. *Chem. Eng. Technol.* **2023**, *46*, 2330–2336.
- (53) Zaykovskaya, A.; Louhi-Kultanen, M. Batch Crystallization of Xylitol by Cooling, Evaporative, and Antisolvent Crystallization. *Cryst. Growth Des.* **2023**, *23*, 1813–1820.
- (54) Kaya, M.; Ceyhan, A. A.; Şahin, O. Effects of different temperatures and additives on the metastable zone width precipitation kinetics of NaBO₂. *Russ. J. Phys. Chem. A* **2014**, *88*, 402–408.
- (55) Habibi, P.; Rahbari, A.; Blazquez, S.; Vega, C.; Dey, P.; Vlught, T. J.; Moulto, O. A. A New Force Field for OH[−] for Computing Thermodynamic and Transport Properties of H₂ and O₂ in Aqueous NaOH and KOH Solutions. *J. Phys. Chem. B* **2022**, *126*, 9376–9387.
- (56) Habibi, P.; Postma, J. R. T.; Padding, J. T.; Dey, P.; Vlught, T. J. H.; Moulto, O. A. Thermodynamic and Transport Properties of H₂/H₂O/NaB(OH)₄ Mixtures Using the Delft Force Field (DFF/B(OH)₄[−]). *Ind. Eng. Chem. Res.* **2023**, *62*, 11992–12005.
- (57) van Rooijen, W. A.; Habibi, P.; Xu, K.; Dey, P.; Vlught, T. J.; Hajibeygi, H.; Moulto, O. A. Interfacial Tensions, Solubilities, and Transport Properties of the H₂/H₂O/NaCl System: A Molecular Simulation Study. *J. Chem. Eng. Data* **2024**, *69*, 307–319.
- (58) Zeron, I. M.; Abascal, J. L. F.; Vega, C. A force field of Li⁺, Na⁺, K⁺, Mg²⁺, Ca²⁺, Cl[−], and SO₄^{2−} in aqueous solution based on the TIP4P/2005 water model and scaled charges for the ions. *J. Chem. Phys.* **2019**, *151*, 134504.
- (59) Núñez-Rojas, E.; González, I.; Guzmán-González, G.; Alejandre, J. Molecular dynamics simulations for liquid electrolytes of propylene carbonate with LiTFSI, LiPF₆, and LiBF₄ salts. *J. Mol. Liq.* **2023**, *390*, 122983.
- (60) Li, P. Phase Behavior and Reaction Mechanism Study of Hydrogen Storage in Sodium Borohydride. Ph.D. Thesis, 2013.
- (61) Ewoldt, R. H.; Johnston, M. T.; Caretta, L. M. In *Complex Fluids in Biological Systems: Experiment, Theory, and Computation*; Spagnolie, S. E., Ed.; Springer New York: New York, NY, 2015; pp 207–241.
- (62) Abascal, J. L. F.; Vega, C. A general purpose model for the condensed phases of water: TIP4P/2005. *J. Chem. Phys.* **2005**, *123*, 234505.
- (63) Tsimpanogiannis, I. N.; Maity, S.; Celebi, A. T.; Moulto, O. A. Engineering Model for Predicting the Intradiusion Coefficients of Hydrogen and Oxygen in Vapor, Liquid, and Supercritical Water based on Molecular Dynamics Simulations. *J. Chem. Eng. Data* **2021**, *66*, 3226–3244.
- (64) Vega, C.; Abascal, J. L. F. Simulating water with rigid non-polarizable models: a general perspective. *Phys. Chem. Chem. Phys.* **2011**, *13*, 19663–19688.
- (65) Vega, C.; de Miguel, E. Surface tension of the most popular models of water by using the test-area simulation method. *J. Chem. Phys.* **2007**, *126*, 154707.
- (66) Tsimpanogiannis, I. N.; Moulto, O. A.; Franco, L. F. M.; Spera, M. B. d. M.; Erdős, M.; Economou, I. G. Self-diffusion coefficient of bulk and confined water: a critical review of classical molecular simulation studies. *Mol. Simul.* **2019**, *45*, 425–453.
- (67) Moulto, O. A.; Tsimpanogiannis, I. N.; Panagiotopoulos, A. Z.; Economou, I. G. Atomistic molecular dynamics simulations of CO₂ diffusivity in H₂O for a wide range of temperatures and pressures. *J. Phys. Chem. B* **2014**, *118*, 5532–5541.
- (68) Döpke, M. F.; Moulto, O. A.; Hartkamp, R. On the transferability of ion parameters to the TIP4P/2005 water model using molecular dynamics simulations. *J. Chem. Phys.* **2020**, *152*, 024501.
- (69) Leontyev, I. V.; Stuchebrukhov, A. A. Electronic Polarizability and the Effective Pair Potentials of Water. *J. Chem. Theory Comput.* **2010**, *6*, 3153–3161.
- (70) Lee, D. Y.; Li, Y. Y.; Noike, T. Continuous H₂ production by anaerobic mixed microflora in membrane bioreactor. *Bioresour. Technol.* **2009**, *100*, 690–695.
- (71) Leontyev, I.; Stuchebrukhov, A. Accounting for electronic polarization in non-polarizable force fields. *Phys. Chem. Chem. Phys.* **2011**, *13*, 2613–2626.
- (72) Li, P.; Henkelman, G.; Keith, J. A.; Johnson, J. K. Elucidation of aqueous solvent-mediated hydrogen-transfer reactions by ab initio molecular dynamics and nudged elastic-band studies of NaBH₄ hydrolysis. *J. Phys. Chem. C* **2014**, *118*, 21385–21399.
- (73) Leontyev, I. V.; Stuchebrukhov, A. A. Polarizable mean-field model of water for biological simulations with AMBER and CHARMM force fields. *J. Chem. Theory Comput.* **2012**, *8*, 3207–3216.
- (74) Leontyev, I. V.; Stuchebrukhov, A. A. Polarizable molecular interactions in condensed phase and their equivalent nonpolarizable models. *J. Chem. Phys.* **2014**, *141*, 014103.
- (75) Martin, M. G.; Siepmann, J. I. Transferable Potentials for Phase Equilibria. 1. United-Atom Description of n-Alkanes. *J. Phys. Chem. B* **1998**, *102*, 2569–2577.
- (76) Frenkel, D.; Smit, B. In *Understanding Molecular Simulation*, 3rd ed.; Frenkel, D., Smit, B., Eds.; Academic Press, 2023.
- (77) Allen, M.; Tildesley, D. *Computer Simulation of Liquids*, 2nd ed.; Oxford Science Publications: Oxford University Press: New York, 2017.
- (78) Plimpton, S. Fast Parallel Algorithms for Short-Range Molecular Dynamics. *J. Comput. Phys.* **1995**, *117*, 1–19.
- (79) Ryckaert, J. P.; Ciccotti, G.; Berendsen, H. J. Numerical integration of the cartesian equations of motion of a system with constraints: molecular dynamics of n-alkanes. *J. Comput. Phys.* **1977**, *23*, 327–341.
- (80) Nguyen, T. D.; Phillips, C. L.; Anderson, J. A.; Glotzer, S. C. Rigid body constraints realized in massively-parallel molecular dynamics on graphics processing units. *Comput. Phys. Commun.* **2011**, *182*, 2307–2313.
- (81) Hockney, W. R.; Eastwood, J. W. *Computer Simulation Using Particles*, 1st ed.; CRC Press: Boca Raton, 1988.
- (82) Luty, B. A.; Davis, M. E.; Tironi, I. G.; Van Gunsteren, W. F. A Comparison of Particle-Particle, Particle-Mesh and Ewald Methods for Calculating Electrostatic Interactions in Periodic Molecular Systems. *Mol. Simul.* **1994**, *14*, 11–20.
- (83) Pollock, E. L.; Glosli, J. Comments on P3M, FMM, and the Ewald method for large periodic Coulombic systems. *Comput. Phys. Commun.* **1996**, *95*, 93–110.
- (84) Verlet, L. Computer “Experiments” on Classical Fluids. I. Thermodynamical Properties of Lennard-Jones Molecules. *Phys. Rev.* **1967**, *159*, 98–103.

- (85) Nosé, S. A unified formulation of the constant temperature molecular dynamics methods. *J. Chem. Phys.* **1984**, *81*, 511–519.
- (86) Hoover, W. G. Canonical dynamics: Equilibrium phase-space distributions. *Phys. Rev. A: At, Mol., Opt. Phys.* **1985**, *31*, 1695–1697.
- (87) Kamberaj, H.; Low, R. J.; Neal, M. P. Time reversible and symplectic integrators for molecular dynamics simulations of rigid molecules. *J. Chem. Phys.* **2005**, *122*, 224114.
- (88) Jamali, S. H.; Wolff, L.; Becker, T. M.; De Groen, M.; Ramdin, M.; Hartkamp, R.; Bardow, A.; Vlugt, T. J.; Moulto, O. A. OCTP: A Tool for On-the-Fly Calculation of Transport Properties of Fluids with the Order- n Algorithm in LAMMPS. *J. Chem. Inf. Model.* **2019**, *59*, 1290–1294.
- (89) Martínez, L.; Andrade, R.; Birgin, E. G.; Martínez, J. M. PACKMOL: A package for building initial configurations for molecular dynamics simulations. *J. Comput. Chem.* **2009**, *30*, 2157–2164.
- (90) Mondello, M.; Grest, G. S. Viscosity calculations of n -alkanes by equilibrium molecular dynamics. *J. Chem. Phys.* **1997**, *106*, 9327–9336.
- (91) Tenney, C.; Maginn, E. Limitations and recommendations for the calculation of shear viscosity using reverse nonequilibrium molecular dynamics. *J. Chem. Phys.* **2010**, *132*, 014103.
- (92) Zwanzig, R. Time-Correlation Functions and Transport Coefficients in Statistical Mechanics. *Annu. Rev. Phys. Chem.* **1965**, *16*, 67–102.
- (93) Jamali, S. H.; Wolff, L.; Becker, T. M.; Bardow, A.; Vlugt, T. J.; Moulto, O. A. Finite-Size Effects of Binary Mutual Diffusion Coefficients from Molecular Dynamics. *J. Chem. Theory Comput.* **2018**, *14*, 2667–2677.
- (94) Celebi, A. T.; Jamali, S. H.; Bardow, A.; Vlugt, T. J. H.; Moulto, O. A. Finite-size effects of diffusion coefficients computed from molecular dynamics: a review of what we have learned so far. *Mol. Simul.* **2021**, *47*, 831–845.
- (95) Jamali, S. H.; Hartkamp, R.; Bardas, C.; Söhl, J.; Vlugt, T. J.; Moulto, O. A. Shear Viscosity Computed from the Finite-Size Effects of Self-Diffusivity in Equilibrium Molecular Dynamics. *J. Chem. Theory Comput.* **2018**, *14*, 5959–5968.
- (96) Moulto, O. A.; Zhang, Y.; Tsimpanogiannis, I. N.; Economou, I. G.; Maginn, E. J. System-size corrections for self-diffusion coefficients calculated from molecular dynamics simulations: The case of CO₂, n -alkanes, and poly(ethylene glycol) dimethyl ethers. *J. Chem. Phys.* **2016**, *145*, 074109.
- (97) Krishna, R.; Van Baten, J. M. The Darken relation for multicomponent diffusion in liquid mixtures of linear alkanes: An investigation using Molecular Dynamics (MD) simulations. *Ind. Eng. Chem. Res.* **2005**, *44*, 6939–6947.
- (98) Liu, X.; Schnell, S. K.; Simon, J.-M.; Krüger, P.; Bedeaux, D.; Kjølstrup, S.; Bardow, A.; Vlugt, T. J. H. Diffusion Coefficients from Molecular Dynamics Simulations in Binary and Ternary Mixtures. *Int. J. Thermophys.* **2013**, *34*, 1169–1196.
- (99) Liu, X.; Schnell, S. K.; Simon, J. M.; Bedeaux, D.; Kjølstrup, S.; Bardow, A.; Vlugt, T. J. Fick diffusion coefficients of liquid mixtures directly obtained from equilibrium molecular dynamics. *J. Phys. Chem. B* **2011**, *115*, 12921–12929.
- (100) Liu, X.; Vlugt, T. J.; Bardow, A. Maxwell-stefan diffusivities in binary mixtures of ionic liquids with dimethyl sulfoxide (DMSO) and H₂O. *J. Phys. Chem. B* **2011**, *115*, 8506–8517.
- (101) Liu, X.; Vlugt, T. J.; Bardow, A. Maxwell–Stefan diffusivities in liquid mixtures: Using molecular dynamics for testing model predictions. *Fluid Phase Equilib.* **2011**, *301*, 110–117.
- (102) Yeh, I.-C.; Hummer, G. System-size dependence of diffusion coefficients and viscosities from molecular dynamics simulations with periodic boundary conditions. *J. Phys. Chem. B* **2004**, *108*, 15873–15879.
- (103) Dünweg, B.; Kremer, K. Molecular dynamics simulation of a polymer chain in solution. *J. Chem. Phys.* **1993**, *99*, 6983–6997.
- (104) Jamali, S. H.; Bardow, A.; Vlugt, T. J.; Moulto, O. A. Generalized Form for Finite-Size Corrections in Mutual Diffusion Coefficients of Multicomponent Mixtures Obtained from Equilibrium Molecular Dynamics Simulation. *J. Chem. Theory Comput.* **2020**, *16*, 3799–3806.
- (105) Delft High Performance Computing Centre (DHPC), DelftBlue Supercomputer (Phase 1). 2022, <https://www.tudelft.nl/dhpc/ark:/44463/DelftBluePhase1> (accessed June 30, 2023).
- (106) Richardson, B. S.; Birdwell, J. F.; Pin, F. G.; Jansen, J. F.; Lind, R. F. Sodium borohydride based hybrid power system. *J. Power Sources* **2005**, *145*, 21–29.
- (107) Joung, I. S.; Cheatham, T. E. Determination of alkali and halide monovalent ion parameters for use in explicitly solvated biomolecular simulations. *J. Phys. Chem. B* **2008**, *112*, 9020–9041.
- (108) Wang, K.; Lu, J.; Zhuang, L. Direct determination of diffusion coefficient for borohydride anions in alkaline solutions using chronoamperometry with spherical Au electrodes. *J. Electroanal. Chem.* **2005**, *585*, 191–196.
- (109) Celebi, A. T.; Vlugt, T. J.; Moulto, O. A. Structural, Thermodynamic, and Transport Properties of Aqueous Reline and Ethaline Solutions from Molecular Dynamics Simulations. *J. Phys. Chem. B* **2019**, *123*, 11014–11025.
- (110) Galliéro, G.; Boned, C.; Baylaucq, A. Molecular dynamics study of the Lennard-Jones fluid viscosity: Application to real fluids. *Ind. Eng. Chem. Res.* **2005**, *44*, 6963–6972.
- (111) Yang, X.; Liu, Q.; Zhang, X.; Ji, C.; Cao, B. A molecular dynamics simulation study of the densities and viscosities of 1,2,4-trimethylbenzene and its binary mixture with n -decane. *Fluid Phase Equilib.* **2022**, *562*, 113566.
- (112) Saric, D.; Kohns, M.; Vrabec, J. Dielectric constant and density of aqueous alkali halide solutions by molecular dynamics: A force field assessment. *J. Chem. Phys.* **2020**, *152*, 164502.
- (113) Guevara-Carrion, G.; Nieto-Draghi, C.; Vrabec, J.; Hasse, H. Prediction of transport properties by molecular simulation: Methanol and their mixture. *J. Phys. Chem. B* **2008**, *112*, 16664–16674.
- (114) Zhang, J.; Fennell, P. S.; Trusler, J. P. M. Density and Viscosity of Partially Carbonated Aqueous Tertiary Alkanolamine Solutions at Temperatures between (298.15 and 353.15) K. *J. Chem. Eng. Data* **2015**, *60*, 2392–2399.
- (115) Patzschke, C. F.; Zhang, J.; Fennell, P. S.; Trusler, J. P. M. Density and Viscosity of Partially Carbonated Aqueous Solutions Containing a Tertiary Alkanolamine and Piperazine at Temperatures between 298.15 and 353.15 K. *J. Chem. Eng. Data* **2017**, *62*, 2075–2083.